JOURNAL OF VIROLOGY, July 2009, p. 7015–7028 Vol. 83, No. 14
0022-538X/09/$08.00+0 doi:10.1128/JVI.00398-09

Onset of Human Cytomegalovirus Replication in Fibroblasts Requires the Presence of an Intact Vimentin Cytoskeleton▽

Matthew S. Miller and Laura Hertel*

Department of Microbiology and Immunology, Schulich School of Medicine and Dentistry, The University of Western Ontario, London, Ontario N6A 5C1, Canada

Received 23 February 2009/Accepted 24 April 2009

Like all viruses, herpesviruses extensively interact with the host cytoskeleton during entry. While microtubules and microfilaments appear to facilitate viral capsid transport toward the nucleus, evidence for a role of intermediate filaments in herpesvirus entry is lacking. Here, we examined the function of vimentin intermediate filaments in fibroblasts during the initial phase of infection of two genotypically distinct strains of human cytomegalovirus (CMV), one with narrow (AD169) and one with broad (TB40/E) cell tropism. Chemical disruption of the vimentin network with acrylamide, intermediate filament bundling in cells from a patient with giant axonal neuropathy, and absence of vimentin in fibroblasts from vimentin$^{-/-}$ mice severely reduced entry of either strain. In vimentin null cells, viral particles remained in the cytoplasm longer than in vimentin$^{+/+}$ cells. TB40/E infection was consistently slower than that of AD169 and was more negatively affected by the disruption or absence of vimentin. These findings demonstrate that an intact vimentin network is required for CMV infection onset, that intermediate filaments may function during viral entry to facilitate capsid trafficking and/or docking to the nuclear envelope, and that maintenance of a broader cell tropism is associated with a higher degree of dependence on the vimentin cytoskeleton.

Human cytomegalovirus (CMV) is a ubiquitous herpesvirus that can cause serious disease in immunocompromised individuals (8, 58). Virtually all cell types, with the exception of lymphocytes and polymorphonuclear leukocytes, can support CMV replication in vivo (80), and this remarkably broad tropism is at the basis of the numerous clinical manifestations of CMV infection (8, 58). The range of permissive cells in vitro is more limited, with human fibroblasts (HF) and endothelial cells being the most widely used for propagation of clinical isolates. Two extensively studied strains, AD169 and Towne, were generated by serial passage of tissue isolates in HF for the purpose of vaccine development (22, 68). During this process, both strains accumulated numerous genomic changes (11) and lost the ability to grow in cell types other than HF. By contrast, propagation in endothelial cells produced strains with more intact genomes and tropism, such as TB40/E, VR1814, TR, and PH (59, 80).

The viral determinants of endothelial and epithelial cell tropism have recently been mapped to the UL128-UL131A (UL128-131A) genomic locus (32, 92, 93). Each of the products of the UL128, UL130, and UL131A genes is independently required for tropism and participates in the formation of a complex at the surface of the virion with the viral glycoproteins gH and gL (74, 93), which can also independently associate with gO (45). The gH/gL/UL128-131A complex appears to be required for entry into endothelial cells by endocytosis, followed by low-pH-dependent fusion of the virus envelope with endosomal membranes (73, 74) although some virus strains expressing the UL128-UL131A genes do not require endosome acidification for capsid release (66, 79).

HF-adapted strains consistently contain mutations in the UL128-131A genes (32). Loss of endothelial cell tropism in AD169 has been associated with a frameshift mutation in the UL131A gene, leading to the production of a truncated protein and to the loss of the gH/gL/UL128-131A complex, but not the gH/gL/gO complex, from the surface of AD169 virions (1, 3, 92). Reestablishment of wild-type UL131A expression in AD169 by repair of the UL131A gene mutation or by *cis*-complementation yielded viruses with restored tropism for endothelial cells but with reduced replication capacities in HF (1, 92). Interestingly, the efficiencies of entry of wild-type and repaired or complemented AD169 viruses were comparable, suggesting that the presence of UL131A did not interfere with the initial steps of infection in HF but negatively affected virion release (1, 92).

The cellular determinants of CMV tropism are numerous and have not been fully identified. Virus entry begins with virion attachment to the ubiquitously expressed heparan sulfate proteoglycans at the cell surface (17), followed by engagement of one or more receptor(s) including the integrin heterodimers $\alpha2\beta1$, $\alpha6\beta1$, and $\alpha_V\beta3$ (23, 39, 94); the platelet-derived growth factor-α receptor (84); and the epidermal growth factor receptor, whose role in CMV entry is still debated (38, 95).

Subsequent delivery of capsids into the cytoplasm requires fusion of the virus envelope with cellular membranes. Release of AD169 capsids in HF occurs mainly by fusion at the plasma membrane at neutral pH although incoming virions have also been found within phagolysosome-like vacuoles (16, 83). Fusion with the plasmalemma appears to be mediated by the gH/gL/gO complex as AD169 virions do not contain the gH/gL/UL128-131A complex, and infectivity of a gO mutant was

* Corresponding author. Mailing address: Department of Microbiology and Immunology, Health Sciences Addition HSA 320, The University of Western Ontario, London, Ontario N6A 5C1, Canada. Phone: (519) 661-4009. Fax: (519) 661-3499. E-mail: lhertel@uwo.ca.
▽ Published ahead of print on 29 April 2009.

severely reduced (37). The mechanism used by strain TB40/E to penetrate into HF has not been described but was assumed to be similar to that of AD169 (80) even though TB40/E virions contain both gH/gL/gO and gH/gL/UL128-131A complexes.

Transport of released, de-enveloped capsids toward the nucleus is mediated by cellular microtubules, and treatment of Towne-infected HF with microtubule-depolymerizing agents substantially reduced expression levels of the viral nuclear immediate-early protein 1 (IE1) (64). Depolymerization of actin microfilaments was also observed in HF as early as 10 to 20 min postinfection with the Towne strain while stress fiber disappearance was evident at 3 to 5 h postinfection (hpi) with AD169 (4, 42, 54), suggesting that microfilament rearrangement may be required to facilitate capsid transition through the actin-rich cell cortex.

The role of intermediate filaments (IF) in CMV infection not been studied. In vivo, expression of the IF protein vimentin is specific to cells of mesenchymal origin like HF and endothelial cells (12). Although the phenotype of vimentin$^{-/-}$ (vim^{-}) mice appears to be mild (15), vimentin-null cells display numerous defects including fragmentation of the Golgi apparatus (26), development of nuclear invaginations in some instances (76), and reduced formation of lipid droplets, glycolipids, and autophagosomes (29, 52, 87). Vimentin IF interact with integrins $\alpha2\beta1$, $\alpha6\beta4$, and $\alpha_V\beta3$ at the cell surface and participate in recycling of integrin-containing endocytic vesicles (40, 41). They also accompany endocytic vesicles during their perinuclear accumulation (34), regulate endosome acidification by binding to the adaptor complex AP-3 (86), control lysosome distribution into the cytoplasm (87), and promote directional mobility of cellular vesicles (69). The vimentin cytoskeleton is tightly associated with the nuclear lamina (10) and was shown to anchor the nucleus within the cell, to mediate force transfer from the cell periphery to the nucleus, and to bind to repetitive DNA sequences as well as to supercoiled DNA and histones in the nuclear matrix (56, 89, 90). Microtubules and vimentin IF form close connections in HF (30). Drug-induced disassembly of the microtubule network alters IF synthesis and organization, leading to the collapse of vimentin IF into perinuclear aggregates (2, 25, 30, 70). By contrast, coiling of IF after injection of antivimentin antibodies has no effect on the structure of microtubules (28, 46, 53), indicating that the interaction between vimentin IF and microtubules is functionally unidirectional.

In this work, we sought to assess the role of the vimentin cytoskeleton in CMV entry. We hypothesized that vimentin association with integrins at the cell surface, with endosomes and microtubules in the cytoplasm, and with the lamina and matrix in the nucleus might facilitate viral binding and penetration, capsid transport toward the nucleus, and nuclear deposition of the viral genome.

We found that, akin to microtubules, vimentin IF do not depolymerize during entry of either AD169 or TB40/E. In comparison to AD169, onset of TB40/E infection in HF was delayed, and the proportion of infected cells was reduced. Virus entry was negatively affected by the disruption of vimentin networks after exposure to acrylamide (ACR), by IF bundling in cells from patients with giant axonal neuropathy (GAN), and by the absence of vimentin IF in vim^{-} mouse embryo fibroblasts (MEF). In vim^{-} cells, the efficiency of particles trafficking toward the nucleus appeared significantly lower than in vimentin$^{+/+}$ (vim^{+}) cells, and in each instance the negative effects were more pronounced in TB40/E-infected cells than in AD169-infected cells. These data show that vimentin is required for efficient entry of CMV into HF and that the endotheliotropic strain TB40/E is more reliant on the presence and integrity of vimentin IF than the HF-adapted strain AD169.

MATERIALS AND METHODS

Cells and virus. Primary foreskin HF (a gift from E. S. Mocarski, Atlanta, GA) were propagated in Dulbecco's modified Eagle medium (DMEM) supplemented with 10% fetal clone serum III (HyClone), 4 mM 4-(2-hydroxyethyl)-1-piperazineethanesulfonic acid (HEPES), 1 mM sodium pyruvate, and 100 U/ml penicillin and 100 μg/ml streptomycin (all from Gibco Invitrogen Corp. [complete DMEM]) and were used between passages 17 and 27 postisolation. Normal dermal HF (MCH070 cells) and dermal HF from a patient with GAN (WG0321 cells) were obtained from the Repository for Mutant Human Cell Strains at Montreal Children's Hospital and were propagated as described above with the addition of 10% fetal bovine serum (HyClone). To induce vimentin IF bundling, cells were cultured in medium lacking serum for 4 days. vim^{+} (MFT-6) and vim^{-} (MFT-16) immortalized MEF (a gift of R. Evans, Aurora, CO) were propagated as described for foreskin HF. Human CMV strains AD169*var*ATCC and TB40/E were kind gifts from E. S. Mocarski and were originally obtained from the ATCC and C. Sinzger (Tübingen, Germany), respectively. Propagation and purification of both strains were performed as described previously (35). Virus titers were determined by plaque assay on HF monolayers in 12-well tissue culture plates. Five different stocks of TB40/E and five of AD169 were used for the experiments described. The identity of each strain was verified by PCR amplification of AD169 and TB40/E genomic extracts with primers mapping to the UL150 gene.

Cell infection. For analysis of microtubules, microfilaments, and vimentin IF structure, HF were plated at a density of 5×10^4 cells/cm^2 in 24-well plates with coverslips 1 day prior to infection with AD169 or TB40/E at a multiplicity of infection (MOI) of 5. Mock-infected samples were exposed to culture medium alone. Cells were harvested at 5 and 30 min (min) postinfection and at 1, 2, and 4 hpi. For expression analyses of IE1 and IE2, HF were plated as above and infected with AD169 or TB40/E at an MOI of 1 or 5 at confluence (3 days postseeding). After adsorption for 1 h, cells were washed twice and incubated in fresh DMEM until 2, 4, 8, 24, 48, 72, and 96 hpi. Endpoint titers of cell-free virus were determined by plaque assay on confluent HF by serial dilution of supernatants from HF infected with AD169 or TB40/E at an MOI of 1 and collected at 24, 48, 72, 96, 120, 144, and 168 hpi. MCH070 and WG0321 cells were seeded in serum-free DMEM at a density of 5×10^4 cells/cm^2 in 24-well plates with coverslips 4 days prior to infection with AD169 or TB40/E at an MOI of 1 or 10. After adsorption for 1 h, cells were washed twice and incubated in fresh DMEM until 4, 8, and 24 hpi. For IE1/IE2 expression analyses, vim^{+} and vim^{-} MEF were seeded at a density of 7.7×10^4 cells/well in 24-well plates with coverslips 1 day prior to infection with AD169 or TB40/E at an MOI of 1 or 10. After adsorption for 1 h, cells were washed twice and incubated in fresh DMEM until 4, 8, and 24 hpi. For pp150 staining analyses, vim^{+} and vim^{-} MEF were prechilled on ice for 20 min before exposure to AD169 or TB40/E virions (MOI of 3) for 1 h on ice. Cells were then transferred to 37°C for 1 h, washed three times with culture medium, and further incubated for 4 and 8 h.

ACR treatment of HF. Confluent HF cultures were exposed for 2, 4, 6, and 8 h to a 5 mM ACR solution made by diluting ACR/bis-ACR solution (30% [wt/vol]; Bio-Rad, Hercules, CA) in culture medium. Uninfected cells were harvested immediately after ACR incubation or after ACR removal, washing, and incubation in fresh medium for 4 h. For infection with AD169 or TB40/E at an MOI of 1 or 5, ACR-pretreated cells were washed, exposed to each virus for 1 h, washed again, and collected at 4 hpi.

Antibodies and immunofluorescence staining analyses. Cells were fixed, permeabilized, and blocked as described previously (36) before incubation with monoclonal antibodies anti-human vimentin (1:200; V9; Santa Cruz Biotechnology, Santa Cruz, CA), anti-α-tubulin (1:100; B-5-1-2; Sigma, St. Louis, MO), anti-pp150 (1:400; originally from W. Britt, Birmingham, AL), or anti-IE1/IE2 (1:500; fluorescein isothiocyanate-conjugated MAb810F; Chemicon, Temecula, CA) for 1 h at room temperature (RT). Samples were then washed in phosphate-buffered saline (PBS)–0.05% Tween-20 and incubated with Alexa Fluor 594-conjugated anti-mouse immunoglobulin G (1:100; Molecular Probes, Eugene,

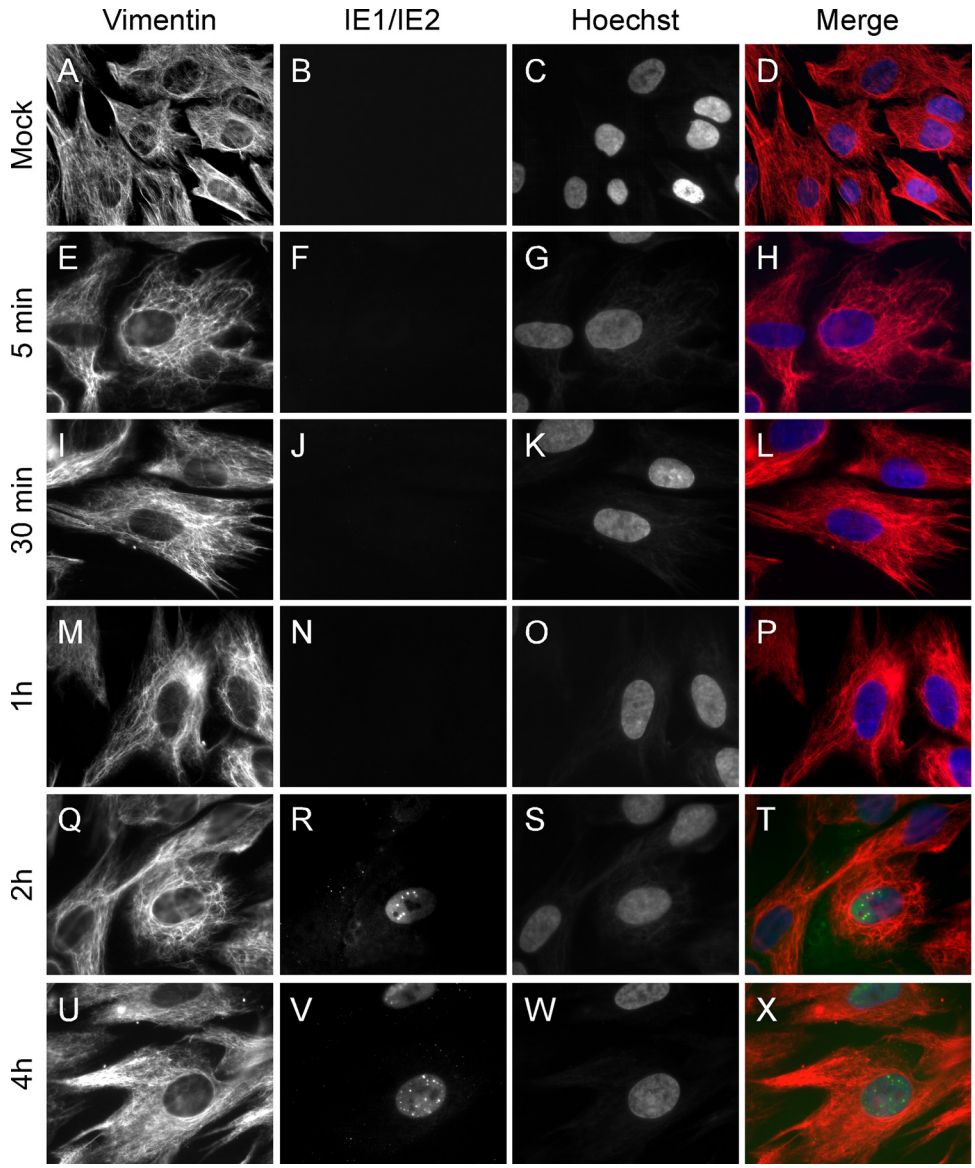

FIG. 1. Organization of the vimentin cytoskeleton during entry of AD169 in HF. Mock-infected (A to D) or AD169-infected (MOI of 5; E to X) HF harvested at 5 or 30 min postinfection and at 1, 2, or 4 hpi were stained with a monoclonal antivimentin antibody followed by an Alexa Fluor 594-conjugated goat anti-mouse antibody (red) and a fluorescein isothiocyanate-conjugated anti-IE1/IE2 antibody (green). Nuclear DNA was highlighted with Hoechst 33342 (blue). Merged images are shown in panels on the right. Original magnification was ×40 for panels A to D and ×100 for panels E to X.

OR) for 1 h at RT. For dual stainings, fixed cells were incubated with a primary antibody and with the Alexa Fluor 594-conjugated goat anti-mouse antibody, blocked with normal mouse immunoglobulin G (1:100; Caltag, Burlingame, CA), and finally stained for IE1/IE2 with MAb810F. Microfilaments were stained with a 1:100 dilution in PBS of Alexa Fluor 568-conjugated phalloidin (Molecular Probes, Eugene, OR), and nuclei were labeled with a 0.2 mg/ml dilution of Hoechst 33342 (Molecular Probes, Eugene, OR) in PBS for 3 min at RT. Coverslips were mounted in 90% glycerol–10% PBS containing 2.5 g/liter of 1, 4 diazabicyclo-(2, 2, 2)-octane (DABCO; Alfa Aesar, Pelham, NH) and analyzed on a Zeiss Axioskop 2 magneto-optical trap fluorescence microscope equipped with a Qimaging Retiga 1300 coded monochrome 12-bit camera. Images were collected and pseudo-colored using Northern Eclipse, version 7.0, software. Confocal images were acquired on a Zeiss LSM 510 META ConfoCor2 laser-scanning confocal microscope equipped with Zeiss LSM 510 META image processing software.

RESULTS

Viral entry does not alter vimentin IF structure. To determine whether the integrity of vimentin IF can impact viral entry, foreskin HF infected with AD169 or TB40/E were harvested at 5 and 30 min and at 1, 2, and 4 hpi; cells were stained with antivimentin and anti-IE1/IE2 antibodies and analyzed by fluorescence microscopy (Fig. 1 and data not shown). In HF infected with AD169 at an MOI of 5, nuclear IE1/IE2 staining was observed in about 10% of the cells as early as at 2 hpi (Fig. 1R), indicating that, by this time, AD169 entry had been successfully completed, with the nuclear deposition of the viral genome and the onset of viral gene synthesis. By contrast,

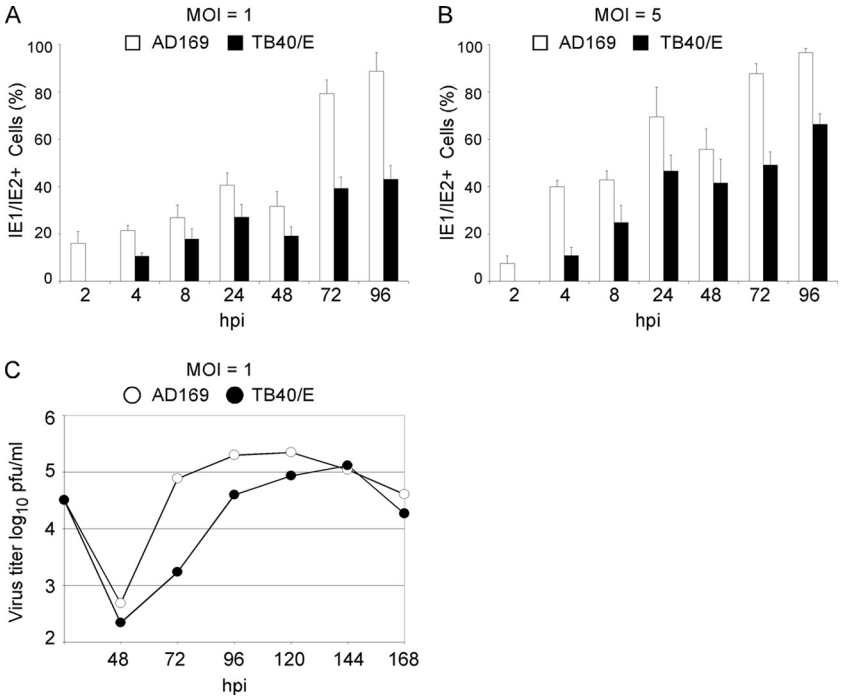

FIG. 2. AD169 and TB40/E infection time course in HF. Cells and supernatants from cultures infected with AD169 or TB40/E at an MOI of 1 (A and C) or 5 (B) were collected at the indicated times postinfection. (A and B) Cells were stained for IE1/IE2, and the percentage of expressing cells was calculated. Means and standard deviations of the percentage values of IE1/IE2-positive cells scored in five separate fields per sample in one representative experiment are shown. (C) Amount of cell-free virus released in supernatants of AD169- and TB40/E-infected HF as quantified by plaque assay.

IE1/IE2 expression was not detected in TB40/E-infected cultures until 4 hpi (data not shown).

In mock-infected cells, vimentin filaments formed a dense, web-like network stretching in all directions toward the cell periphery and forming a border around the nucleus (Fig. 1A to D). Cells infected with AD169 (Fig. 1E to X) or TB40/E (data not shown) exhibited a staining pattern virtually identical to that of mock-infected cells at each of the times tested, suggesting that vimentin IF did not undergo substantial modifications during the initial phase of infection. At later times (24, 72, and 96 hpi), infected cells became rounded and enlarged. Despite these morphological changes, the vimentin perinuclear border and cytoplasmic network remained intact (data not shown).

Parallel sets of samples were also stained for α-tubulin and for actin to determine the effects of viral entry on the structure of microtubules and microfilaments. In AD169 or TB40/E-infected cells, no microtubule disassembly was observed from 5 min to 4 hpi (data not shown), consistent with the role of microtubules in facilitating capsid movement toward the nucleus (64). During infection with AD169, microfilament depolymerization and stress fiber disappearance occurred in 2.6% ± 5% and 35% ± 20% of IE1/IE2-expressing cells at 2 and 4 hpi, respectively. Interestingly, development of this phenotype occurred later and to a lower extent in TB40/E-infected HF, with 5% ± 5% and 7.6% ± 5% of IE1/IE2-positive cells displaying loss of stress fibers at 4 and 8 hpi, respectively.

Together, these results indicate that microtubules and vimentin IF remain structurally intact throughout the initial steps of infection with both strains, suggesting that the integrity of both networks may be required during virus entry. Moreover, onset of replication and microfilament disassembly in TB40/E-infected HF occurred approximately 2 h later than in AD169-infected cells, indicating a potential delay in the initiation of TB40/E infection in HF.

AD169 and TB40/E kinetics of infection in HF are different. To directly compare the growth kinetics of AD169 and TB40/E in HF, confluent cell monolayers were infected in parallel with AD169 or TB40/E at an MOI of 1 or 5. Cells were harvested at 2, 4, 8, 24, 48, 72, and 96 hpi, and IE1/IE2 expression was monitored by immunofluorescence staining analysis. Cell supernatants were also collected at 24, 48, 72, 96, 120, 144, and 168 hpi, and the amount of cell-free virus released during infection was quantified by plaque assay. IE1/IE2 expression was detected in 16% ± 5% (MOI of 1) and in 7.4% ± 3% (MOI of 5) of AD169-infected HF at 2 hpi, with the percentage of positive cells increasing with time up to 89% ± 8% (MOI of 1) and 97% ± 2% (MOI of 5) at 96 hpi (Fig. 2A and B). By contrast, IE1/IE2 expression was not detected at 2 hpi in TB40/E-infected HF (Fig. 2A and B) while at 4 hpi, approximately 10% of infected cells displayed nuclear staining at either MOI. From 4 hpi onwards, the percentage of TB40/E-infected cells increased with time at a rate comparable to that of AD169-infected cells, so that a 1.5- to 2-fold difference in the proportion of AD169- and TB40/E-positive cells was maintained at each time, irrespective of the MOI used.

Consistent with this difference in the number of infected cells, the amount of cell-free virus released in the supernatant of TB40/E-infected cultures was about 100-fold lower than that

released by AD169-infected cells at 72 hpi and about fivefold lower at 96 hpi. At later times, yields became similar, mostly because of the drop in the AD169 virus production (Fig. 2C). These data indicate that the onset of TB40/E infection in HF is delayed compared to AD169 and that the initial difference in the proportion of infected cells is maintained with time. Consequently, TB40/E-infected cells also released smaller amounts of newly formed particles over time.

Pretreatment of HF with ACR inhibits the onset of infection. To determine whether the integrity of the vimentin cytoskeleton is required to facilitate the onset of viral infection, HF were treated with a 5 mM ACR solution for 2, 4, 6, or 8 h prior to infection with either AD169 or TB40/E. ACR is a neurotoxin that has been extensively used to disrupt the organization of IF in neurons and in other cells types (2, 20, 21, 33, 75). ACR treatment of HF induced cell rounding and contraction, accompanied by the aggregation of vimentin IF in elongated bundles extending into the cells' retraction fibers (Fig. 3A to E) (2, 20) and by the appearance of invaginations or folds in the nuclear envelope (Fig. 3F). Consistent with literature reports (20, 47), actin stress fiber disassembly but no microtubule depolymerization was detected in ACR-treated cells (data not shown). As the emergence of nuclear folds has been described to occur in some vimentin null cells, in cells expressing vimentin mutants or containing thick IF bundles, and in ACR-treated neurons (33, 43, 76, 78), we used the percentage of cells with nuclear invaginations as an estimate of the extent of IF disruption. As expected, an exposure time-dependent increase in percentage values was observed, from 1.5% ± 1% after 2 h to 32% ± 7% after 8 h of continual treatment (Fig. 3G). The number of cells displaying nuclear folding became even larger after replacement of ACR with fresh medium for 4 h (Fig. 3G), while incubation in fresh medium for 24 h led to the complete reestablishment of the vimentin IF network and to the disappearance of nuclear invaginations (data not shown), underscoring the reversible nature of ACR-induced changes (2). ACR treatment also did not trigger widespread cell death, as the proportion of cells displaying apoptotic nuclei never increased above 2% (Fig. 3H).

HF pretreated with ACR were infected with AD169 at an MOI of 1 or 5, and the percentage of cells with nuclear invaginations or with apoptotic nuclei at 4 hpi was determined. The extent of nuclear folding in samples infected at either MOI was similar to that of uninfected cells treated with ACR and subsequently incubated for 4 h in fresh medium (Fig. 3, compare panels I and G), suggesting that infection had no effect on the formation of nuclear invaginations. By contrast, a slightly higher fraction of dead cells was found after infection of ACR-treated cells, with the highest value (4.2% ± 3%) observed after 8 h of pretreatment and infection at an MOI of 5 (Fig. 3J).

The proportion of AD169-infected, untreated cells expressing IE1/IE2 was 28% ± 8% at an MOI of 1 and 57% ± 14% at an MOI of 5 (Fig. 4A). ACR pretreatment led to a marked decline in the proportion of IE1/IE2-positive cells. The extent of this decline was dependent on the length of the pretreatment period, with a maximum reduction, relative to untreated samples, of 12-fold (MOI of 1) and 14-fold (MOI of 5) in cells pretreated for 8 h.

The percentage of untreated HF expressing IE1/IE2 after infection with TB40/E was 11% ± 2% at an MOI of 1 and 13% ± 0.2% at an MOI of 5. In cells pretreated with ACR for 6 h, the proportion of IE1/IE2-positive cells had dropped to 0.6% ± 0.9% (19-fold reduction; MOI of 1) and 1.2% ± 1.1% (11-fold reduction; MOI of 5) while in cells pretreated with ACR for 8 h, no IE1/IE2 expression was detected (Fig. 4B).

Thus, pretreatment of HF with ACR significantly inhibited the onset of both AD169 and TB40/E replication.

To assess the reversibility of inhibition, HF were either left untreated or were pretreated with ACR for 4 h prior to ACR removal and exposure to AD169 or TB40/E at an MOI of 1. Removal of the virus inoculum was followed by extensive washing of cells to remove unbound particles and by incubation in fresh medium for 4, 18, and 24 hpi. At 4 hpi, the percentage of IE1/IE2-expressing cells in the pretreated samples was approximately 5-fold (AD169) and 3.5-fold (TB40/E) lower than that of untreated cells at the same time point (Fig. 4C and D). This result was expected, as the vimentin cytoskeleton remains largely disorganized at 4 h after ACR removal (Fig. 3G). However, at 18 and 24 hpi the proportion of IE1/IE2-positive nuclei in ACR-pretreated cells was similar or greater than that of their untreated counterparts, indicating that the block in progression of the infection was removed after the reestablishment of a normal vimentin cytoskeleton.

Vimentin bundling in HF from GAN patients reduces the efficiency of infection. In addition to IF aggregation, ACR treatment of HF also caused stress fiber disassembly (data not shown) and the development of nuclear invaginations (Fig. 3F) and was reported to inhibit protein synthesis (2). Each of these effects might contribute to the observed decrease in the percentage of infected cells. To assess the effects of vimentin IF disruption on viral entry using a different system, we compared the efficiency of onset of AD169 and TB40/E infection in dermal HF harvested from patients with GAN (WG0321 cells) and from healthy control subjects (MCH070 cells).

GAN is a neurodegenerative disorder characterized by bundling of IF in neurons and in other cell types, including HF (67, 96). This phenotype can be conditionally induced in vitro by exposing HF from GAN patients to low-serum conditions (48, 51). Serum starvation for a period of 4 days induced vimentin bundling in 88.8% ± 2.9% of WG0321 cells but did not affect the IF network of MCH070 cells (Fig. 5A to F). IF alteration in WG0321 cells was phenotypically different from that occurring in ACR-treated HF, with the appearance of dense, spherical bundles of vimentin IF in specific areas of the cell and with peripheral filaments and nuclear contacts remaining unperturbed in the majority of the cells. In addition, retraction fibers, nuclear invaginations, and microfilament or microtubule depolymerization were not observed (Fig. 5D to F and data not shown).

Serum-starved WG0321 and MCH070 cells were infected with either AD169 or TB40/E at an MOI of 1 or 10, and the percentage of IE1/IE2-positive cells at 4, 8, and 24 hpi was determined. At 4 hpi, 55% ± 16% (MOI of 1) and 78% ± 12% (MOI of 10) of AD169-infected MCH070 cells showed IE1/IE2 expression (Fig. 5G, H, I, and K). These percentages were slightly higher than those observed at 4 hpi in HF, likely on account of the greater degree of quiescence reached by MCH070 cells after serum starvation. At the same time point, a 3-fold (MOI of 1) and a 1.2-fold (MOI of 10) reduction in the per-

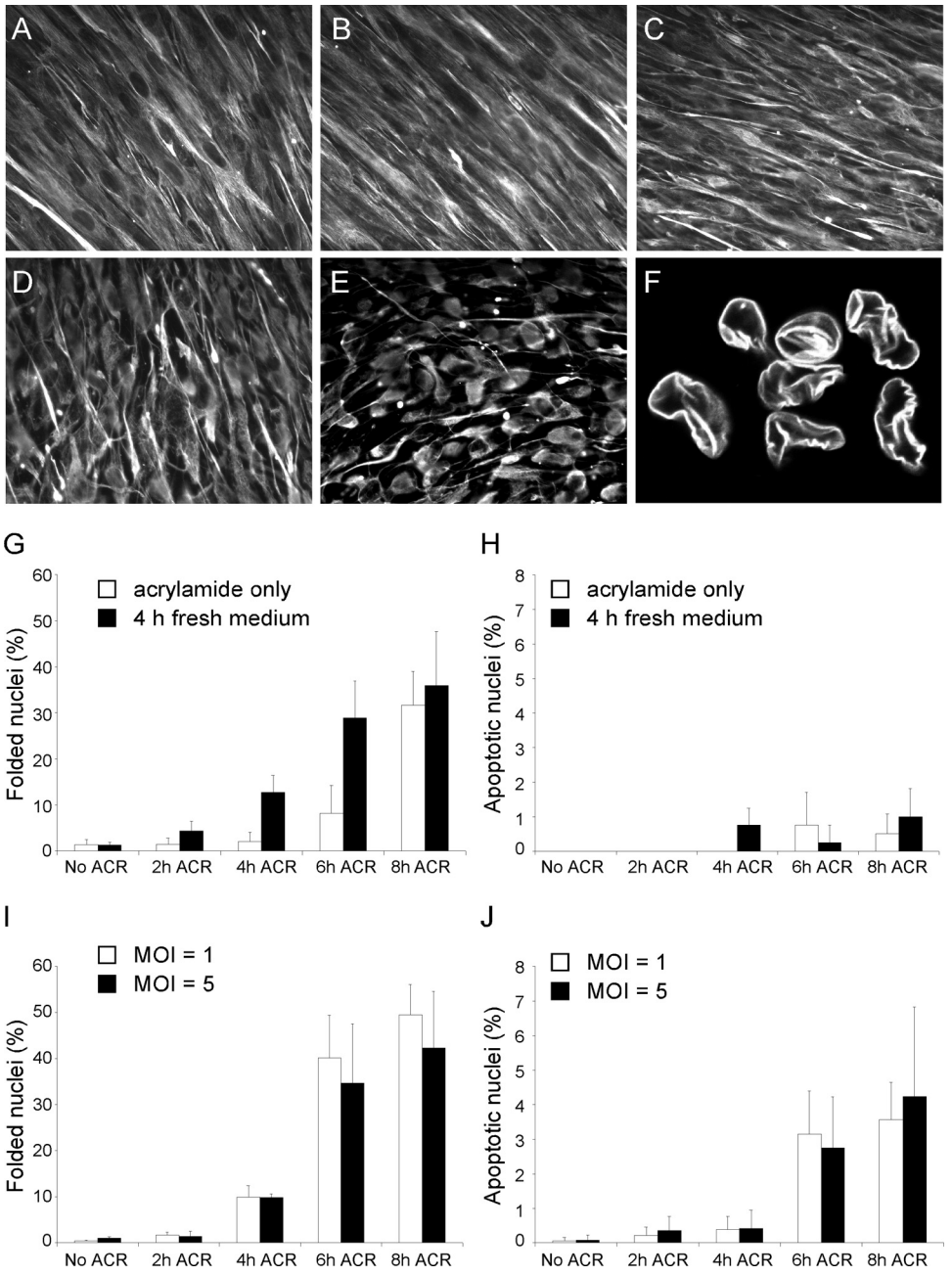

FIG. 3. Effects of ACR pretreatment and AD169 infection on IF organization and nuclear morphology in HF. (A to F) Fluorescence microscopy analysis of vimentin IF organization in untreated HF (A) and in HF exposed to a 5 mM solution of ACR for 2 (B), 4 (C), 6 (D), or 8 h (E) prior to staining with antivimentin antibodies. (F) Confocal microscopy image of lamin B-stained cell nuclei after 6 h of ACR pretreatment. (G and H) Percentage of cells with nuclear invaginations (G) or with nuclear outlines consistent with apoptosis (H) in HF monolayers harvested immediately after ACR treatment for the indicated times (white bars) or harvested after ACR removal and incubation of cells in fresh medium for 4 h (black bars). (I and J) Percentage of cells with nuclear invaginations (I) or with apoptotic nuclei (J) in HF monolayers harvested after ACR treatment for the indicated times and AD169 infection at an MOI of 1 (white bars) or 5 (black bars) for 4 h. Mean and standard deviation values from three independent experiments are shown.

centage of IE1/IE2-positive nuclei was observed in WG0321 cells (Fig. 5I and K). By contrast, at 8 and 24 hpi, WG0321 and MCH070 cell populations contained equal proportions of IE1/IE2-expressing cells at each MOI. These data suggest that vimentin bundling in WG0321 cells may be detrimental to the onset of AD169 replication and that this effect is both MOI and time dependent: smaller differences are observed between the two cell populations after infection at an MOI of 10, and no differences are observed at later time points postinfection.

No IE1/IE2-positive nuclei were detected at 4 hpi in TB40/E-infected WG0321 or MCH070 cells at either MOI (Fig. 5J and L). At 8 and 24 hpi, however, both WG0321 and MCH070

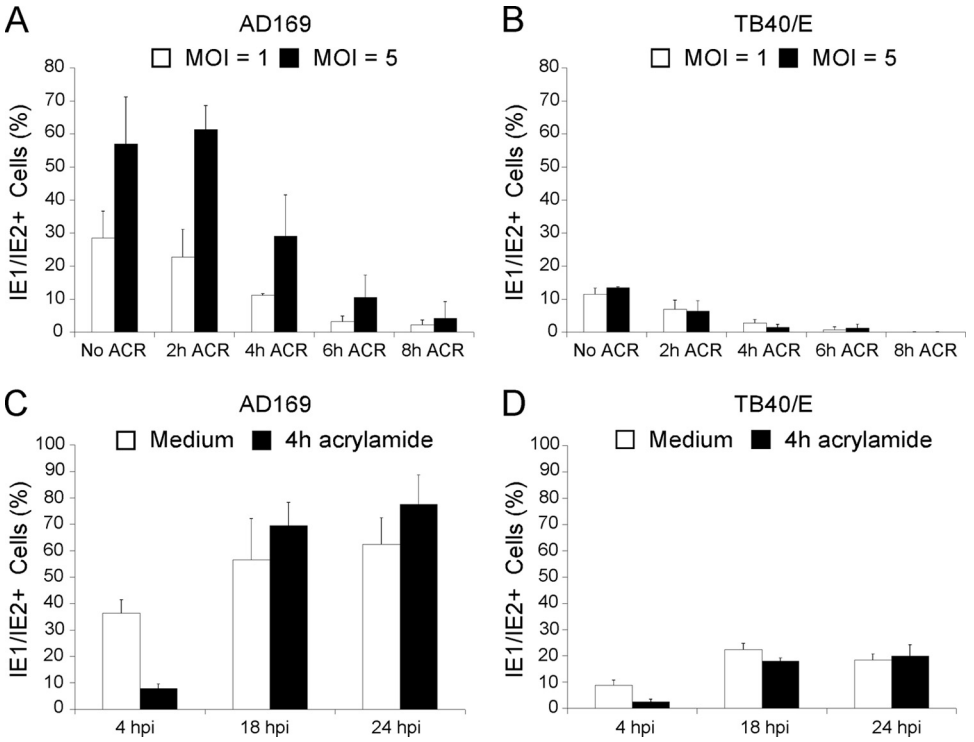

FIG. 4. Impact of ACR pretreatment on AD169 and TB40/E infection efficiency. (A and B) Percentage of IE1/IE2-expressing HF either untreated (No ACR) or after exposure to a 5 mM solution of ACR for 2, 4, 6, or 8 h prior to infection with AD169 or TB40/E at an MOI of 1 or 5 for 4 h. (C and D) Percentage of IE1/IE2-expressing HF left untreated (white bars) or treated with a 5 mM solution of ACR for 4 h (black bars) prior to infection with AD169 or TB40/E at an MOI of 1. Mean and standard deviation values from three (A and C) and two (B and D) independent experiments are shown.

cells expressed IE1/IE2, indicating that initiation of TB40/E replication was delayed but not abrogated. Similar to the situation in HF (Fig. 2A and B), infection of MCH070 with TB40/E yielded approximately 30 to 40% fewer IE1/IE2-positive cells than infection with AD169 at 8 and 24 hpi and at both MOIs, indicating that efficient initiation of TB40/E infection is impaired in HF, regardless of their origin (foreskin or dermis) and of the presence (HF) or absence (MCH070) of serum in the culture medium.

A 1.8-fold reduction in the proportion of IE1/IE2-positive nuclei was observed at 8 h after TB40/E infection of WG0321 cells compared to MCH070 cells, irrespective of the MOI used (Fig. 5J and L). At 24 hpi, the extent of this reduction appeared to decrease slightly to 1.65-fold (MOI of 1) and 1.5-fold (MOI of 10), but was not eliminated as it was for AD169-infected WG0321 cells.

Combined, these data indicate that the presence of vimentin bundles can directly or indirectly impair the efficient onset of both AD169 and TB40/E replication. In contrast to infection with AD169, the degree of impairment of TB40/E infection was MOI independent, and the defect could not be corrected with time.

Absence of vimentin impairs the onset of infection. To further investigate the role of vimentin on virus entry, immortalized vim^+ and vim^- MEF were infected with AD169 or TB40/E at an MOI of 1 or 10, and the proportion of IE1/IE2-positive cells at 4, 8, and 24 hpi was determined. MEF do not support human CMV replication but allow normal entry events to proceed (49, 50), with the block in infection occurring after IE gene expression. Consistent with literature data, IE1/IE2 expression was observed in MEF infected with either strain (Fig. 6), but the percentages of IE1/IE2-positive cells were lower than those found in HF or MCH070 cell populations, possibly as a result of the reduced degree of quiescence reached by immortalized cells compared to primary HF. While the proportion of AD169-infected vim^+ MEF remained unchanged over time, a sudden increase in the number of TB40/E-infected vim^+ MEF was observed between 8 and 24 hpi at each MOI.

At all times tested and at both MOIs, the percentage of IE1/IE2-expressing vim^- MEF infected with AD169 was markedly lower than that observed in vim^+ MEF (Fig. 6 A and C). The largest differences were recorded during infection at an MOI of 1, with fivefold, fourfold, and threefold reductions at 4, 8, and 24 hpi, respectively. At an MOI of 10, differences appeared to be slightly reduced, to an average of 2.3-fold. Interestingly, while the proportion of IE1/IE2-positive, vim^+ cells remained fairly constant (Fig. 6A and C,), the percentage of IE1/IE2-positive, vim^- cells appeared to slowly increase with time at both MOIs (Fig. 6A and C), suggesting that the onset of AD169 infection in vim^- cells was delayed but not abrogated.

Similar to what was observed in HF, the proportion of TB40/E-infected vim^+ cells at either MOI was about three- to fourfold lower than that of AD169-infected vim^+ cells (Fig. 6, compare A to B and C to D). In addition, the absence of vimentin

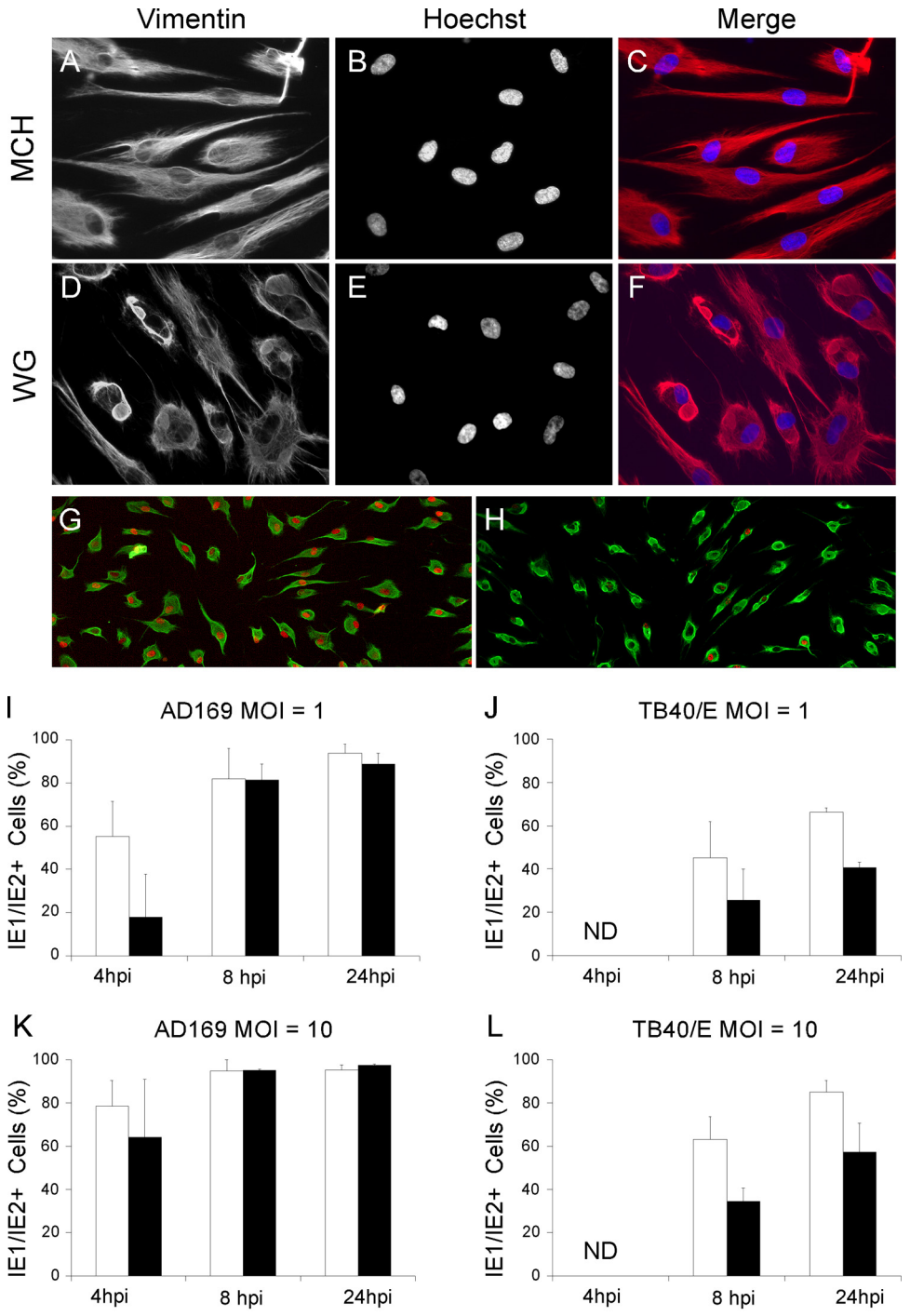

FIG. 5. Structure of vimentin IF and expression of viral IE1/IE2 proteins in WG0321 and WG0321 dermal fibroblasts. (A to F) Serum-starved dermal fibroblasts from healthy donors (MCH070) and from patients with GAN (WG0321) were stained for vimentin and with Hoechst 33342. Merged images are shown as indicated. (G and H) Serum-starved MCH070 (G) and WG0321 (H) dermal fibroblasts were infected with AD169 at an MOI of 10 for 4 h prior to staining for vimentin (green) and for IE1/IE2 (red). (I to L) Percentage of serum-starved MCH070 and WG0321 cells expressing IE1/IE2 after infection with AD169 (I and K) or TB40/E (J and L) at an MOI of 1 or 10. Mean and standard deviation values from three (I, K, and L) and two (J) independent experiments are shown. ND, not detected.

appeared to have a larger impact on the onset of TB40/E infection, with 7- to 9-fold and 3- to 17-fold reductions in the percentages of IE1/IE2-positive vim$^-$ cells observed at an MOI of 1 and 10, respectively (Fig. 6B and D). Finally, and contrary to infection with AD169, the percentages of IE1/IE2-positive vim$^-$ cells appeared to steadily decrease with time during TB40/E infection at both MOIs, an indication of abortive infection.

Together, these data show that the presence of vimentin is

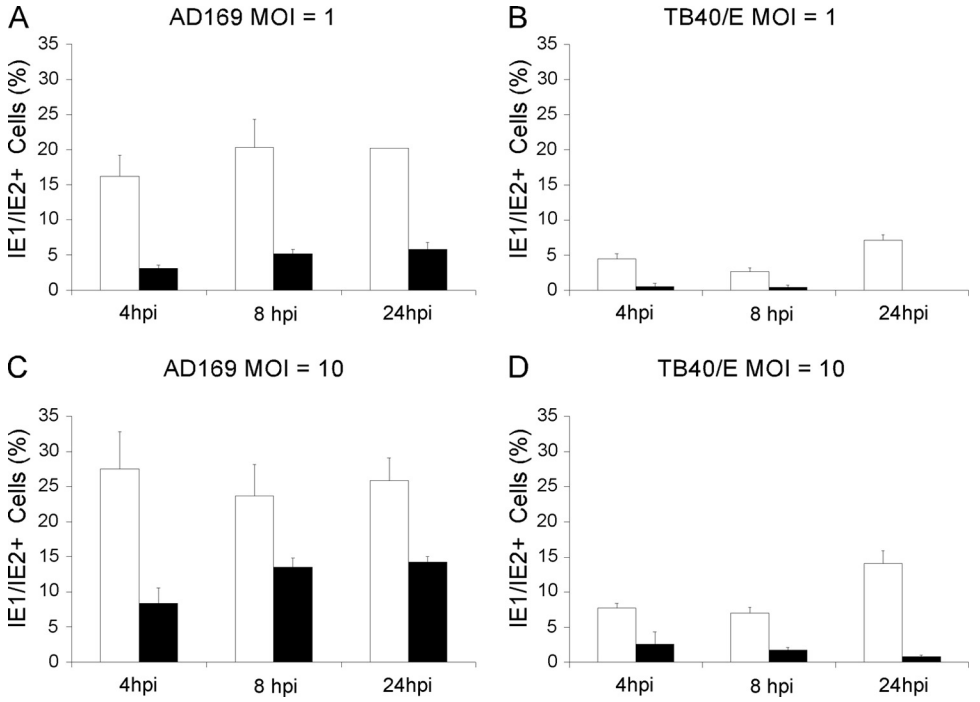

FIG. 6. Viral IE1/IE2 gene expression in vim$^+$ and vim$^-$MEF. Percentage of vim$^+$ (white bars) and vim$^-$ (black bars) MEF expressing IE1/IE2 after infection with AD169 (A and C) or TB40/E (B and D) at an MOI of 1 or 10. Mean and standard deviation values from two independent experiments are shown.

required for the efficient start of both AD169 and TB40/E replication. While onset of AD169 infection in vim$^-$ cells is initially delayed, it appears to recover with time. By contrast, TB40/E infection becomes abortive, suggesting a larger degree of reliance on vimentin for the initial stages of TB40/E infection.

Vimentin is required for proper viral particle trafficking. To assess whether vimentin affected intracellular capsid transport, virion localization was tracked by staining AD169- or TB40/E-infected vim$^+$ and vim$^-$ MEF for pp150, a tegument phosphoprotein that remains strongly associated with capsids during entry and that has been used as capsid marker in other studies (64, 81). At 1 hpi with AD169, the pp150 signal was found predominantly at the cell surface and within the cytoplasm of vim$^+$ and vim$^-$ cells (Fig. 7A and B), and no obvious differences were found between cell types in the total numbers of particles per cell at 1 and 4 hpi. By 8 hpi, only few vim$^+$ cells still contained particles while the pp150 signal was clearly evident in the cytoplasm of several vim$^-$ cells (Fig. 7C and D). The number of pp150-positive, vim$^+$ cells seemed to decline with time much more rapidly than the number of pp150-positive, vim$^-$ cells, suggesting that capsid disassembly and concomitant loss of the pp150 signal might occur more rapidly in the presence of vimentin. To quantify this result, the percentage of pp150-positive vim$^+$ and vim$^-$ MEF was determined after infection with AD169 or TB40/E at an MOI of 3 in synchronized infections. After virus adsorption at 4°C for 1 h, cultures were shifted at 37°C for 1 h to allow for penetration to occur, then washed, and further incubated for 4 and 8 h. The proportions of pp150-positive cells after virus adsorption and penetration were virtually identical in all samples (Fig. 7E), indicating that the absence of vimentin did not affect binding of either strain. After 4 h at 37°C, however, the percentage of pp150-positive vim$^+$ cells infected with AD169 was dramatically lower than that of vim$^-$ cells (Fig. 7E). By 8 h, a slight additional decrease in the percentage of particle-containing cells was observed in vim$^-$ cells (Fig. 7E). In TB40/E-infected cultures, the proportions of virion-containing vim$^+$ and vim$^-$ cells after 1 h at 37°C were almost identical, and no decrease relative to the percentage of pp150-positive cells after virus adsorption for 1 h at 4°C was observed (Fig. 7E). This situation remained unchanged in vim$^-$ MEF until the 8-h time point, when a decrease in the percentage of cells with particles was registered. By contrast, vim$^+$ cultures were characterized by a more gradual decrease in pp150-positive cells over time. Thus, the rate of pp150 signal loss in AD169-infected, vim+ cells was significantly faster than that in TB40/E-infected, vim$^+$ cells, suggesting that AD169 virions may be reaching the nucleus more rapidly than TB40/E virions. To assess if this was indeed the case, the proportion of pp150-positive virions localizing at the cell surface, in the cytoplasm, or in close proximity to the nucleus of infected cells at 1 h posttransfer at 37°C was calculated. In vim$^+$ cells infected with AD169, particles were equally distributed between the cytoplasm and the nucleus while in vim$^-$ cells, virions accumulated in the cytoplasm (Fig. 7F). The majority of virus particles were also found in the cytoplasm of vim$^+$ and vim$^-$ cells infected with TB40/E, supporting the hypothesis of a slower rate of intracellular movement of TB40/E virions than of AD169 virions. In vim$^-$ cells, a slightly higher proportion of TB40/E particles were also observed at the cell periphery, suggesting that penetration of TB40/E capsids may also be delayed by the absence of vimentin.

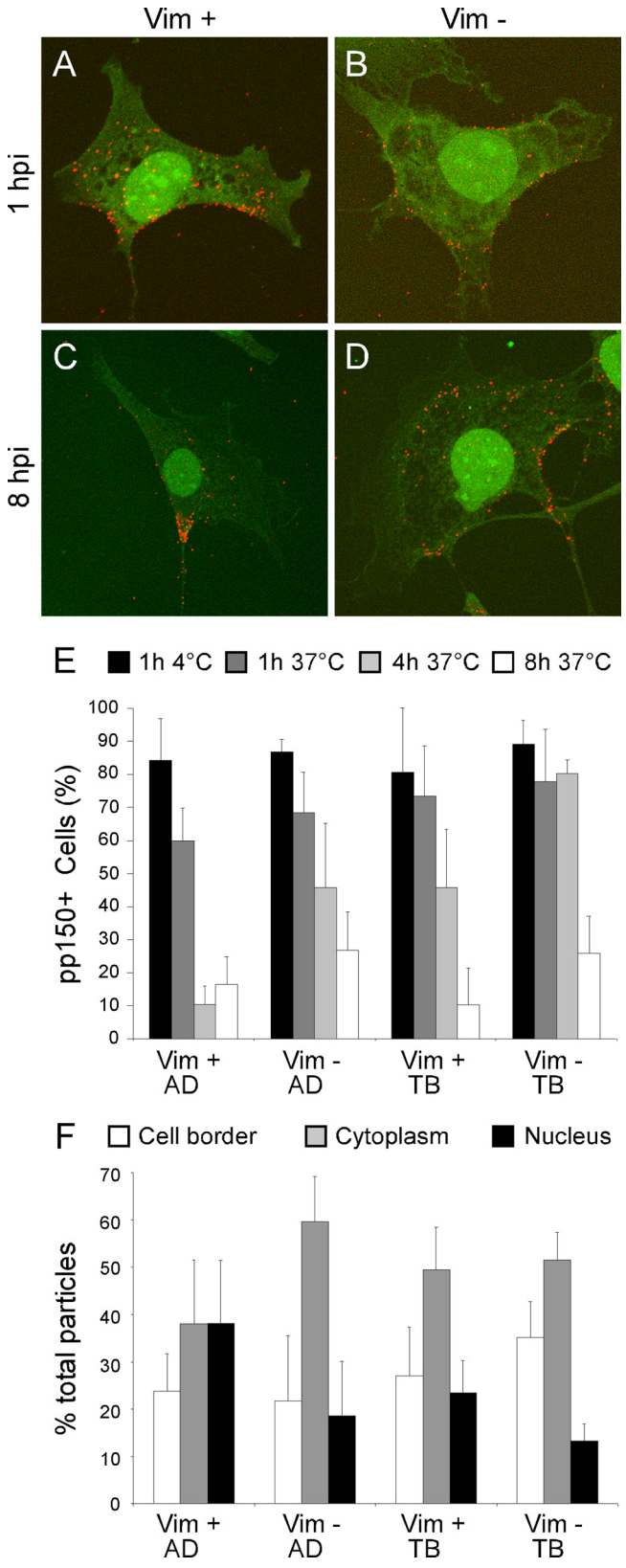

FIG. 7. Detection of virus particles in vim$^+$ and vim$^-$ MEF. (A to D) Confocal immunofluorescence images of AD169-infected MEF stained for pp150 at 1 and 8 hpi. The pp150 signal is depicted in red while the green signal emanates from cellular autofluorescence. (E) Percentage of AD169- and TB40/E-infected vim$^+$ and vim$^-$ MEF containing pp150-positive particles immediately after adsorption (black bars) and at three different times postpenetration (dark gray, light gray, and white bars; times are indicated at the top of the panel). A minimum of 110 cells were counted for each sample. Mean and standard deviation values from separate cell fields in one representative experiment (out of three) are shown. (F) Proportion of pp150-positive particles localizing at the cell surface, in the cytoplasm, or at the nucleus in vim$^+$ and vim$^-$ MEF infected with AD169 or TB40/E at 1 h postpenetration. Mean and standard deviation of values from eight different cells per sample are shown. AD, AD169; TB, TB40/E.

DISCUSSION

During entry, all viruses interact with components of the cellular cytoskeleton to reach their appropriate intracellular sites of replication (71). The role of microfilaments and microtubules in mediating transport of viral particles has been well established for several viruses, including other herpesviruses (31, 55, 71). Although vimentin IF lack polarity and do not directly participate in intracellular cargo movements, they are dynamically integrated with microfilaments and microtubules and are important for infection with a variety of viruses. Expression of vimentin at the cell surface allows for binding and internalization of porcine reproductive and respiratory syndrome virus (44) while its association with capsid components of the human immunodeficiency virus type 1 (88), Theiler's murine encephalomyelitis virus (62), and adenovirus type 2 (5) assists with virus entry. Vimentin was shown to promote assembly of African swine fever virus, frog virus 3, and vaccinia virus by forming protective cage-like structures around the sites of virion production (61, 72, 85), to enhance egress of bluetongue virus particles via interactions with the outer capsid protein VP2 (18), and to be required for Junin virus replication at a stage subsequent to entry but preceding viral protein synthesis (7). A specific role for vimentin in entry of herpesviruses has not been described. Here, we show that vimentin IF are likely to play a role during entry of two CMV strains with different tropisms and that their degree of dependency on an intact vimentin cytoskeleton correlates with the extent of tropism, possibly as a result of different entry mechanisms.

Like all herpesviruses, CMV replicates in the nucleus and requires virions to be actively transferred from the cell membrane to the nuclear envelope at the start of infection. Entry can occur by direct penetration across the plasma membrane or by macropinocytosis, depending on the cell type and the virus strain (16, 79, 83). Both mechanisms require fusion of the virus envelope with cellular lipid bilayers, and the subsequent transport of capsids along cellular microtubules, whose structural integrity is maintained during entry. Consistent with data from Arcangeletti et al. (4), our results show that the vimentin cytoskeleton is not disassembled during the initial steps of CMV infection, suggesting that maintenance of an intact IF network may be necessary for entry. Vimentin disruption and reorganization are induced early during infection with a variety of viruses including reovirus (77), respiratory syncytial virus (27), frog virus 3 (60), Thelier's murine encephalomyelitis virus (62), vaccinia virus (24), and adenovirus types 2, 5, 4, and 9 (6). By contrast, IF connections are preserved in cells infected with herpes simplex virus type 1 (HSV-1) (63), equine herpes virus

type 1 (91) and adenovirus types 3, 7, and 12, whose particles are predominantly found within phagosomes (6), indicating that the requirement for an intact IF cytoskeleton may be shared among different herpesviruses and may be relevant for entry via intracellular vesicles.

In contrast to IF, microfilament disassembly was evident by 2 hpi with AD169 and by 4 hpi with TB40/E. Binding of some herpesviruses to the cell surface triggers rapid reorganization of the actin cytoskeleton (55), and actin depolymerization close to viral particles was observed upon fusion of the Towne envelope with the plasma membrane (42). Microfilament disassembly appeared to be beneficial for the onset of Towne and AD169 infection (4, 42) as it likely facilitated virion transit across the actin-rich cell cortex. By contrast, treatment with actin depolymerizing drugs inhibited uptake of HSV-1 particles in cells where entry by phagocytosis dominated over fusion at the plasma membrane (14), pointing at a possible requirement for intact microfilaments to support myosin VI-mediated transport of endocytic vesicles toward the cell center (9). Thus, the difference we observed between AD169 and TB40/E in the timing of microfilament depolymerization may potentially reflect two different mechanisms of entry of each strain into HF, with fusion at the plasma membrane followed by immediate actin disassembly being predominant for AD169 and endocytosis accompanied by delayed microfilament reorganization being more common for TB40/E. AD169 virions contain the gH/gL/gO complex, which mediates entry by fusion with the plasma membrane, but lack the gH/gL/UL128-131A complex, which is required for entry by endocytosis (73, 74). By contrast, TB40/E virions contain both gH/gL/gO and gH/gL/UL128-131A complexes endowing TB40/E virions with the potential to enter HF either by fusion at the cell surface, by endocytosis, or by a combination of both mechanisms.

Onset of TB40/E infection was delayed by approximately 2 h relative to infection with AD169, and this resulted in a similar delay throughout the time course of infection, with the proportion of IE1/IE2-positive cells in TB40/E-infected monolayers remaining lower than that in AD169-infected cells at each time and irrespective of the MOI used (Fig. 2A and B). These differences are likely to be due to slower and less efficient transport of TB40/E particles, especially if TB40/E entry mechanisms require the generation and intracellular movement of vesicles. Fusion of AD169 virions at the plasma membrane may allow capsids to associate with microtubules in a rapid and efficient manner while escape of TB40/E capsids from endosomes may require longer times. Although the intracellular content of AD169 and TB40/E DNA in HF was reported to be similar at 1.5 hpi (81), HF internalization of radiolabeled AD169 particles was found to be more efficient than that of the clinical strain TR (73). The delay in TB40/E infection onset was also reflected by the lower levels of cell-free virus produced by infected cells at 72, 96, and 120 hpi although by 144 and 168 hpi AD169 and TB40/E yields had equalized (Fig. 2C). To our knowledge, this is the first report directly comparing growth of AD169 and TB40/E in HF. A 10-fold reduction in cell-free virus yields relative to AD169 has been described for another clinical strain, VR1814 (1), while repair or complementation of the UL131A gene mutation in AD169 reduced virus production in HF (1, 92). It is thus conceivable that expression of UL131A might be detrimental for efficient TB40/E production in HF, and additional functions encoded by genes mutated during the process of AD169 adaptation to growth in HF may also contribute to the phenotype we observed.

Previous studies have shown that drug-mediated disassembly of microtubules inhibits onset of infection by CMV (64), HSV-1 (63), and other viruses (31, 57, 71). Microtubules and IF are closely connected; hence, chemical disruption of microtubule networks also invariably leads to changes in the organization of IF, complicating the separation of each system's contribution. To dissect the role of vimentin IF during CMV entry, we determined the efficiency of onset of AD169 and TB40/E infection in fibroblasts with disrupted or absent IF.

ACR has been widely used to selectively and reversibly disrupt vimentin IF without altering microtubule structures (2, 65, 75) and has been employed in studies addressing the role of IF in Junin, bluetongue, and dengue virus replication (7, 13, 18). Treatment of HF with ACR prior to infection with AD169 or TB40/E resulted in an exposure time-dependent decrease in the percentage of infected cells (Fig. 4A and B), suggesting that the integrity of vimentin IF is required for CMV entry. Changes in cell and nuclear morphology and ACR-induced inhibition of protein synthesis may also have contributed to reduce infection rates while the concomitant disassembly of actin stress fibers may have affected the onset of TB40/E, but not of AD169 infection, as microfilament disassembly facilitates entry of AD169 virions (4). By contrast, cell death was not considered to be a significant factor as the percentage of cells with apoptotic nuclei remained consistently low (Fig. 3H and J), and removal of ACR allowed for resumption of infection (Fig. 4C and D). Intriguingly, infection recovery after ACR removal suggests that viral particles are still capable of entering cells with disrupted vimentin IF. Perhaps in the absence of an extended vimentin cytoskeleton, virions remain trapped in the cytoplasm or become unable to deposit the viral genome in nuclei with membrane invaginations. Restoration of a proper IF cytoskeleton accompanied by the disappearance of nuclear folding may then allow for viral particle trafficking and nuclear genome deposition to resume.

To establish the role of vimentin IF during CMV infection in a setting that did not involve exposure to pharmacological agents, IF bundling was induced in fibroblasts from GAN patients by serum starvation. The phenotype of IF in GAN HF cultures was less uniform than that in ACR-treated cultures, with some cells showing more prominent bundling than others and with bundles localizing in distinct areas of each cell, leaving the rest of the IF network fairly intact (Fig. 5F). Inhibition of AD169 infection in this system appeared to be temporary and MOI dependent, which suggests that particles could circumvent the obstacle represented by accumulated IF when given enough time or when present in large amounts. By contrast, TB40/E infection was severely impacted, and the percentage of infected cells did not substantially increase with time or at higher MOIs. These results point again at possible differences in AD169 and TB40/E entry mechanisms. As retrograde transport of endocytic vesicles is severely impaired in neurons from GAN-null mice (19), it is tempting to speculate that transport of CMV particles toward the nucleus may be preferentially delayed in GAN HF if capsids are contained within endosomes rather than free in the cytoplasm following

penetration at the cell surface. A block in the endocytic route of infection is also less likely to be overcome by raising the MOI as the speed and direction of vesicle movements would still remain the limiting factors even in the presence of numerous particles.

Both AD169 and TB40/E were able to infect MEF cells (Fig. 6), but as was observed with HF cultures, the efficiency of onset of TB40/E infection in MEF was lower than that of AD169, pointing at a possible conservation of entry mechanisms between human and mouse HF. While the proportion of AD169-infected vim$^+$ MEF remained stable from 4 to 24 hpi, an increase in the percentage of TB40/E-infected cells was observed at 24 hpi at both MOIs. Intriguingly, the number of vim$^+$ MEF containing AD169 particles decreased very rapidly after penetration was allowed to proceed and remained stable later on while the reduction in the number of TB40/E-positive cells occurred much more gradually (Fig. 7). Combined, these results suggest that entry of AD169 is more rapid and efficient that that of TB40/E, with prompt capsid trafficking and nuclear genome translocation occurring in the majority of AD169-infected cells. By contrast, cytoplasmic movement of TB40/E virions is lengthier, and, perhaps as a result of this delay, the percentage of cells expressing IE1/IE2 increases only at later times in infection. Initiation of infection with both strains in vim$^-$ MEF is dramatically hampered, particularly at low MOIs, demonstrating that this protein is required for infection. Intriguingly, although the absence of vimentin seemed to only reduce the speed of AD169 particle translocation, it effectively blocked progression of TB40/E virions. Consequently, the proportion of AD169-infected vim$^-$ cells still increased over time while TB40/E infection became abortive, perhaps as a result of virion degradation in the cytoplasm. Viral DNA was indeed reported to be eliminated from the cytoplasm of endothelial cells as a consequence of failures in particle transport toward the nucleus and in nuclear genome deposition (82).

In summary, the efficiency of onset of CMV infection depends on the presence and integrity of the vimentin cytoskeleton, which may facilitate virus entry at different steps. As the proportions of vim$^+$ and vim$^-$pp150-positive cells were similar, a role for vimentin as a CMV receptor at the cell surface is unlikely (Fig. 8, step a). Likewise, participation of IF in uncoating of clathrin from endocytic vesicles (86) is not expected to impact CMV entry (Fig. 8, step b), as clathrin-coated endosomes are too small to accommodate CMV virions (79). By contrast, vimentin could promote capsid binding to microtubules after entry at the plasma membrane (Fig. 8, step c), enhance internalization of endocytic vesicles carrying virions bound to integrins (Fig. 8, step d), or allow for rapid AP-3-mediated acidification of endosomes and concomitant intracytoplasmic release of endocytosed virions (Fig. 8, step e). Finally, vimentin interactions with the nuclear lamina (10) and with cellular DNA (89, 90) may increase the speed of viral genome translocation across the nuclear envelope and of IE gene transcription (Fig. 8, step f). Additional work will be needed to pinpoint the exact steps during viral entry that require vimentin assistance. Based on the differences we observed between AD169 and TB40/E, these will likely depend on the mechanisms of virus entry and will require the engagement of different virion components encoded by each strain.

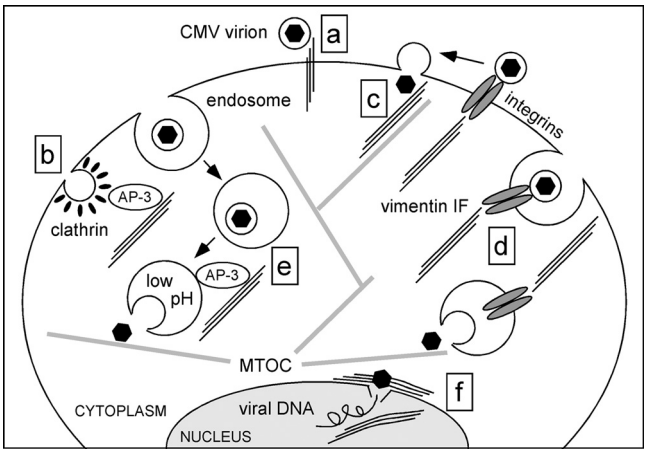

FIG. 8. Hypothetical steps during CMV entry requiring vimentin assistance for efficient completion. Vimentin IF and microtubules are shown as three parallel thin lines and as thick gray lines, respectively. Black hexagons enclosed in a circle depict enveloped virions while isolated black hexagons represent virus capsids. Steps are as follows: (a) vimentin IF acting as receptors for CMV virions at the surface, (b) AP-3-mediated involvement of vimentin IF in internalization of clathrin-coated endosomes, (c) enhancement of capsid attachment and movement along microtubules via vimentin IF, (d) internalization of integrin-bound virions under the control of vimentin IF, (e) AP-3-mediated involvement of vimentin IF in endosome acidification and cytoplasmic release of capsids, and (f) facilitation of nuclear genome deposition and of gene transcription onset by nuclear lamina- and matrix-associated vimentin. MTOC, microtubule organizing center.

ACKNOWLEDGMENTS

This investigation was supported by operating grants to L.H. from the Canadian Institutes of Health Research and from the Natural Sciences and Engineering Research Council.

We are grateful to R. Evans for the donation of mouse embryo fibroblasts from vimentin$^{-/-}$ and vimentin$^{+/+}$ mice and to E. S. Mocarski and J. Mymryk for critical reading of the manuscript.

REFERENCES

1. **Adler, B., L. Scrivano, Z. Ruzcics, B. Rupp, C. Sinzger, and U. Koszinowski.** 2006. Role of human cytomegalovirus UL131A in cell type-specific virus entry and release. J. Gen. Virol. **87:**2451–2460.
2. **Aggeler, J., and K. Seely.** 1990. Cytoskeletal dynamics in rabbit synovial fibroblasts. I. Effects of acrylamide on intermediate filaments and microfilaments. Cell Motil. Cytoskeleton **16:**110–120.
3. **Akter, P., C. Cunningham, B. P. McSharry, A. Dolan, C. Addison, D. J. Dargan, A. F. Hassan-Walker, V. C. Emery, P. D. Griffiths, G. W. Wilkinson, and A. J. Davison.** 2003. Two novel spliced genes in human cytomegalovirus. J. Gen. Virol. **84:**1117–1122.
4. **Arcangeletti, M. C., F. Pinardi, M. C. Medici, E. Pilotti, F. De Conto, F. Ferraglia, M. P. Landini, C. Chezzi, and G. Dettori.** 2000. Cytoskeleton involvement during human cytomegalovirus replicative cycle in human embryo fibroblasts. New Microbiol. **23:**241–256.
5. **Belin, M. T., and P. Boulanger.** 1985. Cytoskeletal proteins associated with intracytoplasmic human adenovirus at an early stage of infection. Exp. Cell Res. **160:**356–370.
6. **Belin, M. T., and P. Boulanger.** 1987. Processing of vimentin occurs during the early stages of adenovirus infection. J. Virol. **61:**2559–2566.
7. **Bhattacharya, B., R. J. Noad, and P. Roy.** 2007. Interaction between Bluetongue virus outer capsid protein VP2 and vimentin is necessary for virus egress. Virol. J. **4:**7.
8. **Britt, W.** 2008. Manifestations of human cytomegalovirus infection: proposed mechanisms of acute and chronic disease. Curr. Top. Microbiol. Immunol. **325:**417–470.
9. **Buss, F., G. Spudich, and J. Kendrick-Jones.** 2004. Myosin VI: cellular functions and motor properties. Annu. Rev. Cell Dev. Biol. **20:**649–676.

10. **Capco, D. G., K. M. Wan, and S. Penman.** 1982. The nuclear matrix: three-dimensional architecture and protein composition. Cell **29:**847–858.
11. **Cha, T. A., E. Tom, G. W. Kemble, G. M. Duke, E. S. Mocarski, and R. R. Spaete.** 1996. Human cytomegalovirus clinical isolates carry at least 19 genes not found in laboratory strains. J. Virol. **70:**78–83.
12. **Chang, L., and R. D. Goldman.** 2004. Intermediate filaments mediate cytoskeletal crosstalk. Nat. Rev. Mol. Cell Biol. **5:**601–613.
13. **Chen, W., N. Gao, J. L. Wang, Y. P. Tian, Z. T. Chen, and J. An.** 2008. Vimentin is required for dengue virus serotype 2 infection but microtubules are not necessary for this process. Arch. Virol. **153:**1777–1781.
14. **Clement, C., V. Tiwari, P. M. Scanlan, T. Valyi-Nagy, B. Y. Yue, and D. Shukla.** 2006. A novel role for phagocytosis-like uptake in herpes simplex virus entry. J. Cell Biol. **174:**1009–1021.
15. **Colucci-Guyon, E., M. M. Portier, I. Dunia, D. Paulin, S. Pournin, and C. Babinet.** 1994. Mice lacking vimentin develop and reproduce without an obvious phenotype. Cell **79:**679–694.
16. **Compton, T., R. R. Nepomuceno, and D. M. Nowlin.** 1992. Human cytomegalovirus penetrates host cells by pH-independent fusion at the cell surface. Virology **191:**387–395.
17. **Compton, T., D. M. Nowlin, and N. R. Cooper.** 1993. Initiation of human cytomegalovirus infection requires initial interaction with cell surface heparan sulfate. Virology **193:**834–841.
18. **Cordo, S. M., and N. A. Candurra.** 2003. Intermediate filament integrity is required for Junin virus replication. Virus Res. **97:**47–55.
19. **Ding, J., E. Allen, W. Wang, A. Valle, C. Wu, T. Nardine, B. Cui, J. Yi, A. Taylor, N. L. Jeon, S. Chu, Y. So, H. Vogel, R. Tolwani, W. Mobley, and Y. Yang.** 2006. Gene targeting of GAN in mouse causes a toxic accumulation of microtubule-associated protein 8 and impaired retrograde axonal transport. Hum. Mol. Genet. **15:**1451–1463.
20. **Durham, H. D., S. D. Pena, and S. Carpenter.** 1983. The neurotoxins 2,5-hexanedione and acrylamide promote aggregation of intermediate filaments in cultured fibroblasts. Muscle Nerve **6:**631–637.
21. **Eckert, B. S.** 1985. Alteration of intermediate filament distribution in PtK1 cells by acrylamide. Eur. J. Cell Biol. **37:**169–174.
22. **Elek, S. D., and H. Stern.** 1974. Development of a vaccine against mental retardation caused by cytomegalovirus infection in utero. Lancet **1:**1–5.
23. **Feire, A. L., H. Koss, and T. Compton.** 2004. Cellular integrins function as entry receptors for human cytomegalovirus via a highly conserved disintegrin-like domain. Proc. Natl. Acad. Sci. USA **101:**15470–15475.
24. **Ferreira, L. R., N. Moussatche, and V. Moura Neto.** 1994. Rearrangement of intermediate filament network of BHK-21 cells infected with vaccinia virus. Arch. Virol. **138:**273–285.
25. **Franke, W. W., E. Schmid, M. Osborn, and K. Weber.** 1978. Different intermediate-sized filaments distinguished by immunofluorescence microscopy. Proc. Natl. Acad. Sci. USA **75:**5034–5038.
26. **Gao, Y., and E. Sztul.** 2001. A novel interaction of the Golgi complex with the vimentin intermediate filament cytoskeleton. J. Cell Biol. **152:**877–894.
27. **Garcia-Barreno, B., J. L. Jorcano, T. Aukenbauer, C. Lopez-Galindez, and J. A. Melero.** 1988. Participation of cytoskeletal intermediate filaments in the infectious cycle of human respiratory syncytial virus (RSV). Virus Res. **9:**307–321.
28. **Gawlitta, W., M. Osborn, and K. Weber.** 1981. Coiling of intermediate filaments induced by microinjection of a vimentin-specific antibody does not interfere with locomotion and mitosis. Eur. J. Cell Biol. **26:**83–90.
29. **Gillard, B. K., R. Clement, E. Colucci-Guyon, C. Babinet, G. Schwarzmann, T. Taki, T. Kasama, and D. M. Marcus.** 1998. Decreased synthesis of glycosphingolipids in cells lacking vimentin intermediate filaments. Exp. Cell Res. **242:**561–572.
30. **Goldman, R. D.** 1971. The role of three cytoplasmic fibers in BHK-21 cell motility. I. Microtubules and the effects of colchicine. J. Cell Biol. **51:**752–762.
31. **Greber, U. F., and M. Way.** 2006. A superhighway to virus infection. Cell **124:**741–754.
32. **Hahn, G., M. G. Revello, M. Patrone, E. Percivalle, G. Campanini, A. Sarasini, M. Wagner, A. Gallina, G. Milanesi, U. Koszinowski, F. Baldanti, and G. Gerna.** 2004. Human cytomegalovirus UL131-128 genes are indispensable for virus growth in endothelial cells and virus transfer to leukocytes. J. Virol. **78:**10023–10033.
33. **Hay, M., and U. De Boni.** 1991. Chromatin motion in neuronal interphase nuclei: changes induced by disruption of intermediate filaments. Cell Motil. Cytoskeleton. **18:**63–75.
34. **Herman, B., and D. F. Albertini.** 1982. The intracellular movement of endocytic vesicles in cultured granulosa cells. Cell Motil. **2:**583–597.
35. **Hertel, L., V. G. Lacaille, H. Strobl, E. D. Mellins, and E. S. Mocarski.** 2003. Susceptibility of immature and mature Langerhans cell-type dendritic cells to infection and immunomodulation by human cytomegalovirus. J. Virol. **77:**7563–7574.
36. **Hertel, L., and E. S. Mocarski.** 2004. Global analysis of host cell gene expression late during cytomegalovirus infection reveals extensive dysregulation of cell cycle gene expression and induction of pseudomitosis independent of US28 function. J. Virol. **78:**11988–12011.
37. **Hobom, U., W. Brune, M. Messerle, G. Hahn, and U. H. Koszinowski.** 2000. Fast screening procedures for random transposon libraries of cloned herpesvirus genomes: mutational analysis of human cytomegalovirus envelope glycoprotein genes. J. Virol. **74:**7720–7729.
38. **Isaacson, M. K., A. L. Feire, and T. Compton.** 2007. Epidermal growth factor receptor is not required for human cytomegalovirus entry or signaling. J. Virol. **81:**6241–6247.
39. **Isaacson, M. K., L. K. Juckem, and T. Compton.** 2008. Virus entry and innate immune activation. Curr. Top. Microbiol. Immunol. **325:**85–100.
40. **Ivaska, J., H. M. Pallari, J. Nevo, and J. E. Eriksson.** 2007. Novel functions of vimentin in cell adhesion, migration, and signaling. Exp. Cell Res. **313:**2050–2062.
41. **Ivaska, J., K. Vuoriluoto, T. Huovinen, I. Izawa, M. Inagaki, and P. J. Parker.** 2005. PKε-mediated phosphorylation of vimentin controls integrin recycling and motility. EMBO J. **24:**3834–3845.
42. **Jones, N. L., J. C. Lewis, and B. A. Kilpatrick.** 1986. Cytoskeletal disruption during human cytomegalovirus infection of human lung fibroblasts. Eur. J. Cell Biol. **41:**304–312.
43. **Kamei, H.** 1994. Relationship of nuclear invaginations to perinuclear rings composed of intermediate filaments in MIA PaCa-2 and some other cells. Cell Struct. Funct. **19:**123–132.
44. **Kim, J. K., A. M. Fahad, K. Shanmukhappa, and S. Kapil.** 2006. Defining the cellular target(s) of porcine reproductive and respiratory syndrome virus blocking monoclonal antibody 7G10. J. Virol. **80:**689–696.
45. **Kinzler, E. R., R. N. Theiler, and T. Compton.** 2002. Expression and reconstitution of the gH/gL/gO complex of human cytomegalovirus. J. Clin. Virol. **25**(Suppl. 2)**:**S87–S95.
46. **Klymkowsky, M. W.** 1981. Intermediate filaments in 3T3 cells collapse after intracellular injection of a monoclonal anti-intermediate filament antibody. Nature **291:**249–251.
47. **Klymkowsky, M. W.** 1988. Metabolic inhibitors and intermediate filament organization in human fibroblasts. Exp. Cell Res. **174:**282–290.
48. **Klymkowsky, M. W., and D. J. Plummer.** 1985. Giant axonal neuropathy: a conditional mutation affecting cytoskeletal organization. J. Cell Biol. **100:**245–250.
49. **LaFemina, R. L., and G. S. Hayward.** 1988. Differences in cell-type-specific blocks to immediate early gene expression and DNA replication of human, simian and murine cytomegalovirus. J. Gen. Virol. **69:**355–374.
50. **LaFemina, R. L., and G. S. Hayward.** 1983. Replicative forms of human cytomegalovirus DNA with joined termini are found in permissively infected human cells but not in non-permissive Balb/c-3T3 mouse cells. J. Gen. Virol. **64:**373–389.
51. **Leung, C. L., Y. Pang, C. Shu, D. Goryunov, and R. K. Liem.** 2007. Alterations in lipid metabolism gene expression and abnormal lipid accumulation in fibroblast explants from giant axonal neuropathy patients. BMC Genet. **8:**6.
52. **Lieber, J. G., and R. M. Evans.** 1996. Disruption of the vimentin intermediate filament system during adipose conversion of 3T3-L1 cells inhibits lipid droplet accumulation. J. Cell Sci. **109:**3047–3058.
53. **Lin, J. J., and J. R. Feramisco.** 1981. Disruption of the in vivo distribution of the intermediate filaments in fibroblasts through the microinjection of a specific monoclonal antibody. Cell **24:**185–193.
54. **Losse, D., R. Lauer, D. Weder, and K. Radsak.** 1982. Actin distribution and synthesis in human fibroblasts infected by cytomegalovirus. Arch. Virol. **71:**353–359.
55. **Lyman, M. G., and L. W. Enquist.** 2009. Herpesvirus interactions with the host cytoskeleton. J. Virol. **83:**2058–2066.
56. **Maniotis, A. J., C. S. Chen, and D. E. Ingber.** 1997. Demonstration of mechanical connections between integrins, cytoskeletal filaments, and nucleoplasm that stabilize nuclear structure. Proc. Natl. Acad. Sci. USA **94:**849–854.
57. **Marsh, M., and A. Helenius.** 2006. Virus entry: open sesame. Cell **124:**729–740.
58. **Mocarski, E. S., T. Shenk, and R. F. Pass.** 2007. Cytomegaloviruses, p. 2701–2772. *In* D. M. Knipe, P. M. Howley, D. E. Griffin, R. A. Lamb, M. A. Martin, B. Roizman, and S. E. Straus (ed.), Fields virology, 5th ed. Lippincott Williams & Wilkins, Philadelphia, PA.
59. **Murphy, E., and T. Shenk.** 2008. Human cytomegalovirus genome. Curr. Top. Microbiol. Immunol. **325:**1–19.
60. **Murti, K. G., and R. Goorha.** 1983. Interaction of frog virus-3 with the cytoskeleton. I. Altered organization of microtubules, intermediate filaments, and microfilaments. J. Cell Biol. **96:**1248–1257.
61. **Murti, K. G., R. Goorha, and M. W. Klymkowsky.** 1988. A functional role for intermediate filaments in the formation of frog virus 3 assembly sites. Virology **162:**264–269.
62. **Nedellec, P., P. Vicart, C. Laurent-Winter, C. Martinat, M. C. Prevost, and M. Brahic.** 1998. Interaction of Theiler's virus with intermediate filaments of infected cells. J. Virol. **72:**9553–9560.
63. **Norrild, B., V. P. Lehto, and I. Virtanen.** 1986. Organization of cytoskeleton elements during herpes simplex virus type 1 infection of human fibroblasts: an immunofluorescence study. J. Gen. Virol. **67:**97–105.
64. **Ogawa-Goto, K., K. Tanaka, W. Gibson, E. Moriishi, Y. Miura, T. Kurata,**

S. Irie, and T. Sata. 2003. Microtubule network facilitates nuclear targeting of human cytomegalovirus capsid. J. Virol. **77:**8541–8547.
65. **Olink-Coux, M., M. Huesca, and K. Scherrer.** 1992. Specific types of prosomes are associated to subnetworks of the intermediate filaments in PtK1 cells. Eur. J. Cell Biol. **59:**148–159.
66. **Patrone, M., M. Secchi, E. Bonaparte, G. Milanesi, and A. Gallina.** 2007. Cytomegalovirus UL131-128 products promote gB conformational transition and gB-gH interaction during entry into endothelial cells. J. Virol. **81:**11479–11488.
67. **Pena, S. D.** 1981. Giant axonal neuropathy: intermediate filament aggregates in cultured skin fibroblasts. Neurology **31:**1470–1473.
68. **Plotkin, S. A., T. Furukawa, N. Zygraich, and C. Huygelen.** 1975. Candidate cytomegalovirus strain for human vaccination. Infect. Immun. **12:**521–527.
69. **Potokar, M., M. Kreft, L. Li, J. Daniel Andersson, T. Pangrsic, H. H. Chowdhury, M. Pekny, and R. Zorec.** 2007. Cytoskeleton and vesicle mobility in astrocytes. Traffic **8:**12–20.
70. **Prahlad, V., M. Yoon, R. D. Moir, R. D. Vale, and R. D. Goldman.** 1998. Rapid movements of vimentin on microtubule tracks: kinesin-dependent assembly of intermediate filament networks. J. Cell Biol. **143:**159–170.
71. **Radtke, K., K. Dohner, and B. Sodeik.** 2006. Viral interactions with the cytoskeleton: a hitchhiker's guide to the cell. Cell Microbiol. **8:**387–400.
72. **Risco, C., J. R. Rodriguez, C. Lopez-Iglesias, J. L. Carrascosa, M. Esteban, and D. Rodriguez.** 2002. Endoplasmic reticulum-Golgi intermediate compartment membranes and vimentin filaments participate in vaccinia virus assembly. J. Virol. **76:**1839–1855.
73. **Ryckman, B. J., M. A. Jarvis, D. D. Drummond, J. A. Nelson, and D. C. Johnson.** 2006. Human cytomegalovirus entry into epithelial and endothelial cells depends on genes UL128 to UL150 and occurs by endocytosis and low-pH fusion. J. Virol. **80:**710–722.
74. **Ryckman, B. J., B. L. Rainish, M. C. Chase, J. A. Borton, J. A. Nelson, M. A. Jarvis, and D. C. Johnson.** 2008. Characterization of the human cytomegalovirus gH/gL/UL128-131 complex that mediates entry into epithelial and endothelial cells. J. Virol. **82:**60–70.
75. **Sager, P. R.** 1989. Cytoskeletal effects of acrylamide and 2,5-hexanedione: selective aggregation of vimentin filaments. Toxicol. Appl. Pharmacol. **97:**141–155.
76. **Sarria, A. J., J. G. Lieber, S. K. Nordeen, and R. M. Evans.** 1994. The presence or absence of a vimentin-type intermediate filament network affects the shape of the nucleus in human SW-13 cells. J. Cell Sci. **107:**1593–1607.
77. **Sharpe, A. H., L. B. Chen, and B. N. Fields.** 1982. The interaction of mammalian reoviruses with the cytoskeleton of monkey kidney CV-1 cells. Virology **120:**399–411.
78. **Shoeman, R. L., C. Huttermann, R. Hartig, and P. Traub.** 2001. Amino-terminal polypeptides of vimentin are responsible for the changes in nuclear architecture associated with human immunodeficiency virus type 1 protease activity in tissue culture cells. Mol. Biol. Cell **12:**143–154.
79. **Sinzger, C.** 2008. Entry route of HCMV into endothelial cells. J. Clin. Virol. **41:**174–179.
80. **Sinzger, C., M. Digel, and G. Jahn.** 2008. Cytomegalovirus cell tropism. Curr. Top. Microbiol. Immunol. **325:**63–83.
81. **Sinzger, C., M. Kahl, K. Laib, K. Klingel, P. Rieger, B. Plachter, and G. Jahn.** 2000. Tropism of human cytomegalovirus for endothelial cells is determined by a post-entry step dependent on efficient translocation to the nucleus. J. Gen. Virol. **81:**3021–3035.
82. **Slobbe-van Drunen, M. E., A. T. Hendrickx, R. C. Vossen, E. J. Speel, M. C. van Dam-Mieras, and C. A. Bruggeman.** 1998. Nuclear import as a barrier to infection of human umbilical vein endothelial cells by human cytomegalovirus strain AD169. Virus Res. **56:**149–156.
83. **Smith, J. D., and E. de Harven.** 1974. Herpes simplex virus and human cytomegalovirus replication in WI-38 cells. II. An ultrastructural study of viral penetration. J. Virol. **14:**945–956.
84. **Soroceanu, L., A. Akhavan, and C. S. Cobbs.** 2008. Platelet-derived growth factor-alpha receptor activation is required for human cytomegalovirus infection. Nature **455:**391–395.
85. **Stefanovic, S., M. Windsor, K. I. Nagata, M. Inagaki, and T. Wileman.** 2005. Vimentin rearrangement during African swine fever virus infection involves retrograde transport along microtubules and phosphorylation of vimentin by calcium calmodulin kinase II. J. Virol. **79:**11766–11775.
86. **Styers, M. L., A. P. Kowalczyk, and V. Faundez.** 2005. Intermediate filaments and vesicular membrane traffic: the odd couple's first dance? Traffic **6:**359–365.
87. **Styers, M. L., G. Salazar, R. Love, A. A. Peden, A. P. Kowalczyk, and V. Faundez.** 2004. The endo-lysosomal sorting machinery interacts with the intermediate filament cytoskeleton. Mol. Biol. Cell **15:**5369–5382.
88. **Thomas, E. K., R. J. Connelly, S. Pennathur, L. Dubrovsky, O. K. Haffar, and M. I. Bukrinsky.** 1996. Anti-idiotypic antibody to the V3 domain of gp120 binds to vimentin: a possible role of intermediate filaments in the early steps of HIV-1 infection cycle. Viral Immunol. **9:**73–87.
89. **Tolstonog, G. V., E. Mothes, R. L. Shoeman, and P. Traub.** 2001. Isolation of SDS-stable complexes of the intermediate filament protein vimentin with repetitive, mobile, nuclear matrix attachment region, and mitochondrial DNA sequence elements from cultured mouse and human fibroblasts. DNA Cell Biol. **20:**531–554.
90. **Traub, P.** 1995. Intermediate filaments and gene regulation. Physiol. Chem. Phys Med. NMR **27:**377–400.
91. **Walter, I., and N. Nowotny.** 1999. Equine herpes virus type 1 (EHV-1) infection induces alterations in the cytoskeleton of Vero cells but not apoptosis. Arch. Virol. **144:**1827–1836.
92. **Wang, D., and T. Shenk.** 2005. Human cytomegalovirus UL131 open reading frame is required for epithelial cell tropism. J. Virol. **79:**10330–10338.
93. **Wang, D., and T. Shenk.** 2005. Human cytomegalovirus virion protein complex required for epithelial and endothelial cell tropism. Proc. Natl. Acad. Sci. USA **102:**18153–18158.
94. **Wang, X., D. Y. Huang, S. M. Huong, and E. S. Huang.** 2005. Integrin $\alpha v\beta 3$ is a coreceptor for human cytomegalovirus. Nat. Med. **11:**515–521.
95. **Wang, X., S. M. Huong, M. L. Chiu, N. Raab-Traub, and E. S. Huang.** 2003. Epidermal growth factor receptor is a cellular receptor for human cytomegalovirus. Nature **424:**456–461.
96. **Yang, Y., E. Allen, J. Ding, and W. Wang.** 2007. Giant axonal neuropathy. Cell Mol. Life Sci. **64:**601–609.